ACCSCIENCE PUBLISHING

International Journal of Bioprinting

RESEARCH ARTICLE

Generative design of patient-specific bone plates for Schatzker type VI tibial plateau fractures

Weiting Xu[1], Xiaoqiang Zheng[2], Yan Xu[1], Rixiang Quan[1], Yi Huang[1], Weiqiang Li[3], Cian Vyas[4], Paulo Bartolo[4,5], Di Wang[2], and Fengyuan Liu[1]*

[1]School of Electrical, Electronic, and Mechanical Engineering, University of Bristol, Bristol, United Kingdom

[2]School of Mechanical & Automotive Engineering, South China University of Technology, Guangzhou, Guangdong, China

[3]Shenzhen Jinshi 3D Printing Technology Co., Ltd., Shenzhen, Guangdong, China

[4]Singapore Centre for 3D Printing, Nanyang Technological University, Singapore

[5]School of Mechanical and Aerospace Engineering, Nanyang Technological University, Singapore

Abstract

Schatzker type VI fractures are complex tibial plateau injuries characterized by multiple fracture lines and complete separation between the plateau and the shaft. These features reduce the effectiveness of standard commercial fixation plates, which often fail to conform to the irregular anatomy. Patient-specific plates, tailored to individual bone geometry, offer improved anatomical fit and fixation. This study aims to compare two patient-specific designs, based on 3D reconstruction (3DP) and generative design (GDP), with a conventional commercial plate (CP). To enable rapid and cost-effective evaluation, all designs were first prototyped in poly(lactic acid) using fused deposition modeling. In bending tests, both 3DP and GDP were significantly stiffer than CP, with stiffness increases of 23.8% and 10.0%, respectively. In biomechanical compression tests, both patient-specific designs exhibited approximately 15% lower displacement than CP under a 750 N load. Based on these results, the GDP design was selected for metal additive manufacturing using laser powder bed fusion. The metal-printed GDP was tested under a compressive load of 750 N and showed a mean displacement of 2.11 ± 0.01 mm, remaining below the commonly accepted clinical threshold of 3 mm. This work highlights the potential of combining PLA-based prototyping with targeted metal validation to support surgical decision-making and streamline implant development.

***Keywords*:** 3D printing; generative design; patient-specific bone plate; Schatzker type VI fractures

***Corresponding author:**
Fengyuan Liu
(fengyuan.liu@bristol.ac.uk)

Citation: Xu W, Zheng X, Xu Y, *et al.* Generative design of patient-specific bone plate for Schatzker type VI tibial plateau fractures. *Int J Bioprint.* 2026;12(1):559-575. doi: 10.36922/IJB025400410

Received: October 2, 2025
Revised: October 29, 2025
Accepted: November 4, 2025
Published online: November 4, 2025

1. Introduction

Schatzker type VI tibial fractures, also classified as *Arbeitsgemeinschaft für Osteosynthesefragen*/Orthopedic Trauma Association 41-C fractures, are among the most severe and complex types of tibial plateau fractures.[1,2] These fractures account for 23% of complex tibial plateau injuries and occur in 1–2% of all fractures, with an overall incidence of 51.7 per 100,000 individuals each year, based on a 10-year epidemiological

study from the Swedish Fracture Register.[3–6] They involve multiple parts of the tibia, including the lateral and medial tibial plateaus, the metaphysis, and the diaphysis. This damage results in a complete separation between the joint surface and the tibial shaft, causing significant instability,[7] as illustrated in Figure 1A.

The primary cause of these fractures is high-energy trauma, such as motor vehicle accidents or falls from significant heights.[8] In addition to bone damage, these injuries are often associated with soft tissue injuries and ligament tears due to the force of impact. Because the fracture lines extend into the joint, treatment must address both joint stability and load-bearing capacity. Furthermore, the complex anatomical geometry of these fractures poses significant challenges to effective treatment and healing. Without timely and appropriate intervention, patients face a high risk of complications, including infection, malunion, nonunion, and post-traumatic osteoarthritis.[9]

Surgical intervention is crucial for managing Schatzker type VI fractures, with the primary goals of stabilizing the fracture, restoring joint function, and minimizing long-term complications. Treating these complex fractures often involves a variety of tools. External devices, such as external fixators, are frequently used for initial stabilization, while circular wire fixators can provide additional support to the diaphyseal region when necessary. Internal tools, including intramedullary nailing, K-wires for provisional alignment, and bone grafts for filling bone defects, are commonly employed to address specific fracture components.[10,11] Considering the high biomechanical load conditions of the knee joint, open reduction and internal fixation with bone

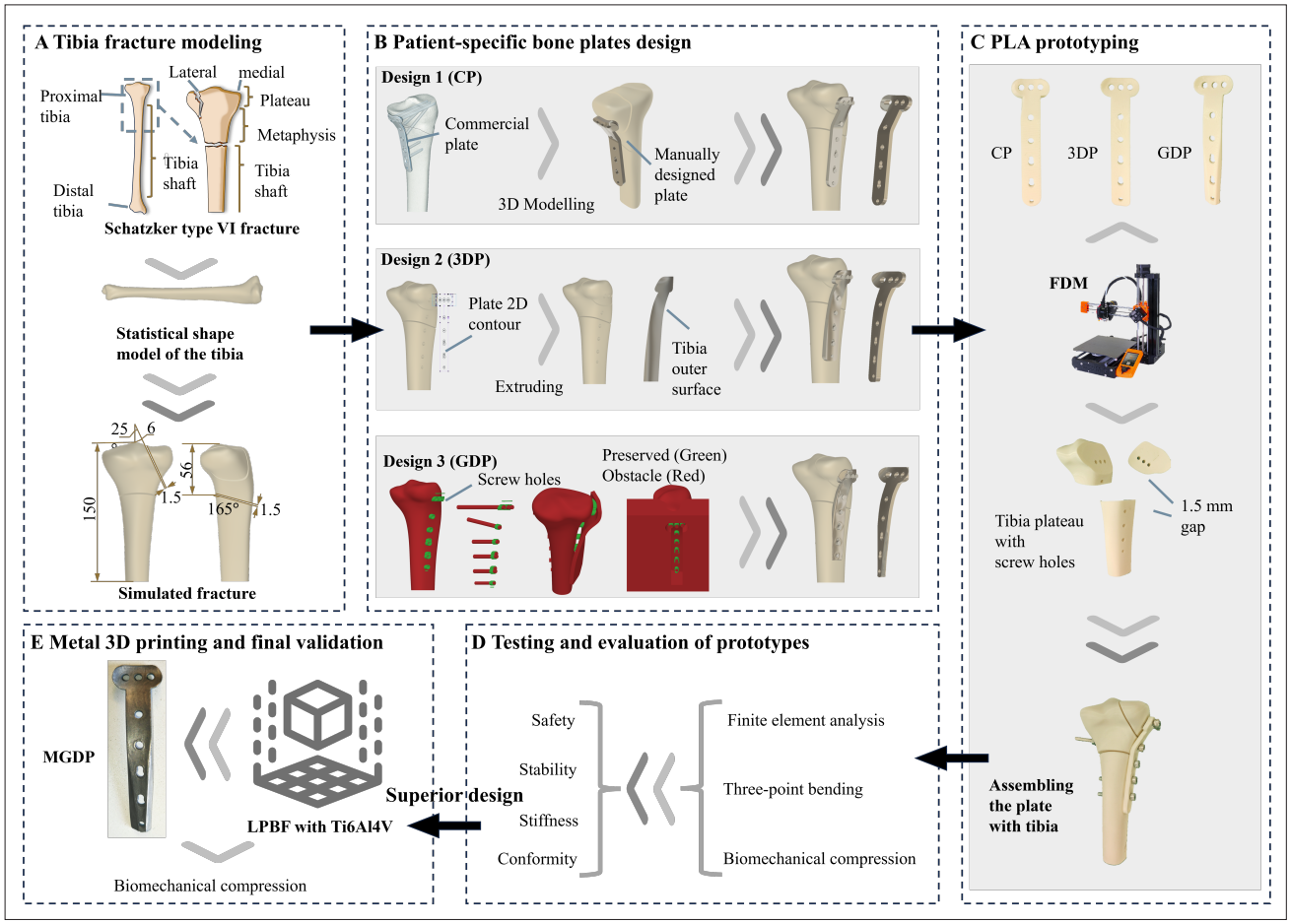

Figure 1. Workflow of the study: (A) Simulation of a Schatzker type VI fracture with a 1.5 mm gap; (B) Design of the baseline plate (CP) and patient-specific bone plates 3DP and GDP; (C) Fabrication of PLA prototypes using FDM; (D) Mechanical and biomechanical testing of the prototypes; (E) Metal additive manufacturing of the GDP using LPBF followed by biomechanical testing. Abbreviations: CP, commercial plate; FDM, fused deposition modeling; GDP, generatively designed patient-specific bone plate; LPBF, laser powder bed fusion; MGDP, metal generatively designed bone plate; PLA, poly(lactic acid); 3DP, 3D reconstruction design plate.

plates and screw systems remains the most common and widely adopted approach.[12]

Bone plates, typically made of biomedical metal materials such as 316L stainless steel or titanium alloys due to their superior mechanical properties, play a critical role in restoring joint alignment and stability while bearing the load required for early mobilization.[13] Despite their critical role, standard bone plates have limitations. They may not precisely conform to the unique anatomical structure of each patient, potentially leading to improper fixation or loosening of the plate or screws, which may require revision surgery.[14,15] Additionally, standard plates carry the risk of stress shielding, in which the plate bears too much load, reducing stress on the bone and increasing the risk of healing complications or deformities.[16,17] These limitations highlight the need for improved designs tailored to individual patients to optimize outcomes in the treatment of Schatzker type VI fractures.

Recently, the development of patient-specific bone plates has become increasingly common, driven by advancements in metal additive manufacturing (AM).[18] These plates are primarily created using 3D reconstruction methods, which enable precise customization for individual fracture sites by integrating advanced scanning technologies and collaborative designs between engineers and surgeons.[19] For instance, Teo *et al.*[20] designed a patient-specific bone plate for lateral tibial plateau fractures that was produced using selective laser melting with 316L stainless steel in 24–29 hours. This turnaround time enabled implantation before the onset of bone healing, thereby reducing the risk of complications associated with prolonged immobility. Similarly, Tilton *et al.*[21] demonstrated that AM-centric fixation designs for patient-specific plates reduced average varus collapse (medial fracture gap displacement) by 47.2% and the risk of screw cut-out by 14.6% compared to conventional plate designs. However, applying metal AM in biomedical implant design presents several challenges. Most patient-specific plates are produced using laser powder bed fusion (LPBF), a technique that involves high equipment and material costs.[22] In addition, extensive post-processing—such as support removal, machining, polishing, and heat treatment—is often required to ensure surface quality, dimensional accuracy, and biocompatibility.[23] These steps are time-consuming and add significant complexity, especially in the early design phase when multiple iterations are typically needed.

Alternatively, generative design (GD) has emerged as a transformative approach for patient-specific bone plate design, attracting growing research attention. This artificial intelligence (AI)-assisted methodology iteratively generates diverse design solutions based on predefined constraints and objectives, enabling precise and optimized outcomes.[24] Baumgartner *et al.*[25] applied GD to develop bridging plates for mandibular bone defects in dogs, achieving superior mechanical performance compared to traditional designs. Kanagalingam *et al.*[26] further demonstrated the potential of GD for high tibial osteotomy plates, designing and fabricating plates using electron beam melting. The success of this study demonstrates that GD, when combined with AM, offers a promising approach for patient-specific implant development. By leveraging AI to generate personalized and biomechanically optimized solutions, this method has the potential to significantly reduce design time and eliminate the iterative communication between surgeons and engineers during the design cycle. Recent work has begun to extend GD from planar parts to anatomically complex implants and fixation devices. Cheng *et al.*[27] proposed a semi-automated GD workflow in Fusion 360 for orthognathic plates, reporting shorter hands-on design time and acceptable stress levels for titanium hardware. Dewey *et al.*[28] combined GD-architected Voronoi meshes with mineralized collagen to produce trim-to-fit craniofacial composites that conform to irregular defects while maintaining predictable stiffness. Alvarado-Moreno *et al.*[29] used GD to reconstruct mandibular continuity after tumor resection, balancing mass and rigidity and verifying mechanical response with finite element analysis for polymer implants secured by titanium or stainless-steel hardware. However, most existing studies focus on implants subjected to limited or simplified loading conditions rather than realistic load-bearing scenarios. This indicates that the full potential of GD has yet to be realized, particularly for bone plates that experience complex, multi-directional forces, such as those in proximal tibia fixation. Further research is required to enhance GD's capability to model and optimize designs under physiological load conditions for clinically relevant and load-bearing applications.

This study focuses on designing patient-specific bone plates for Schatzker type VI fractures using 3D reconstruction and GD and comparing their performance with commercial plates (CPs) through biomechanical experimental tests. To facilitate rapid design validation, the patient-specific plates are initially fabricated using fused deposition modeling (FDM) with poly(lactic acid) (PLA), allowing cost-effective prototyping and experimental verification of mechanical property trends. Based on these evaluations, selected designs are further manufactured in Ti6Al4V using LPBF for definitive biomechanical testing. The findings from this study aim to provide a thorough assessment of patient-specific plate designs and contribute to the optimization of treatment strategies for managing complex tibial fractures.

2. Materials and methods

2.1. Base tibia model and Schatzker type VI tibial fracture simulation

In this study, the open-access statistical shape models (SSMs) of the tibia developed by Keast *et al.*[30] were utilized as the foundation for design (Figure 1A). These models were generated from computed tomography scans of 30 cadavers (20 male, 10 female) sourced from the New Mexico Decedent Image Database. Keast *et al.*[30] employed segmentation and reconstruction of both cortical and trabecular structures of the tibia and fibula. Principal component analysis was applied to capture 95% of the geometric variation present within the dataset, resulting in anatomically accurate and statistically robust tibial representations. Although an SSM is generated from a population dataset, it can still support patient-specific design by statistically representing anatomical variations across individuals.[31,32] By fitting or sampling the model to approximate a given morphology, it provides a realistic surrogate of a patient's tibia when direct imaging data are unavailable.[33] This allows the design workflow, optimization, and validation processes to be developed and tested under anatomically credible conditions consistent with patient-specific design principles. For this study, the mean tibia shape model was exported in Standard Tessellation Language (STL) format and imported into Autodesk Fusion 360 v2.0 (Autodesk Inc., United States of America). This workflow ensured precise control over tibial shape and geometry during the design process. The design focused on a plate for proximal tibia fixation, particularly addressing lateral tibial plateau involvement.

The fracture simulation, crucial for evaluating the designed bone plate, was conducted in Autodesk Fusion 360 v2.0 (Autodesk Inc., United States of America) using the imported tibia model, as shown in Figure 1A. According to the Schatzker classification, type VI fractures are characterized by complete dissociation between the metaphysis and diaphysis of the tibia, often with significant articular involvement and extensive comminution of the lateral tibial plateau. To replicate this fracture pattern, the proximal 150 mm of the tibia was segmented to simulate articular-diaphyseal separation.

In fracture fragment reduction, a 0 mm gap is ideal, as it ensures absolute stability and direct bone healing. However, in complex fractures such as Schatzker type VI, achieving complete fragment contact is often impractical due to comminution and anatomical constraints. Clinically, fracture gaps during surgery typically range from 0 to 3 mm, with gaps exceeding 2 mm being associated with delayed union and increased nonunion risk. Studies indicate that a controlled 1.5 mm gap provides a balance between mechanical stability and biological stimulation, allowing sufficient micromotion for callus formation while avoiding excessive strain.[34–38]

In this study, the fracture gaps were carefully designed to simulate a clinically relevant Schatzker type VI fracture while ensuring accurate analysis of the mechanical behavior of the fixation. A 1.5 mm gap was introduced 56 mm from the proximal end of the tibia, extending through the shaft and separating the plateau from the tibial body at an angle of 15°. Furthermore, a 25° inclined gap, offset 6 mm from the central axis of the lateral tibial plateau, was created to replicate the typical lateral disruption observed in type VI fractures, as illustrated in Figure 1A. These fracture configurations were modeled in Fusion 360 v2.0 (Autodesk Inc., United States of America), ensuring an anatomically accurate representation of the injury.

2.2. Bone plate design

2.2.1. Commercial plate design (baseline)

The design for the comparison group was created to align with the simulated fracture's position and size, ensuring consistency with the anatomical and mechanical requirements of the study. Using Autodesk Fusion 360 v2.0 (Autodesk Inc., United States of America), the implant geometry was replicated from the DePuy Synthes Locking Compression Plate (LCP) Periarticular Plating System, specifically the 4.5 mm thickness LCP Medial Proximal Tibia Plate (DePuy Synthes, United States of America).[39] This plate, designed for the right tibia, features four main holes and measures 106 mm in length. The resulting design, referred to as the comparison CP, was modeled to match the geometry and specifications of the original plate as accurately as possible, ensuring it could serve as a reference for evaluating the patient-specific design. The final design of the CP is shown in Figure 1B, illustrating its structure and alignment with the original implant specifications.

2.2.2. Patient-specific plate design based on 3D reconstruction

In this study, the 3D reconstructed patient-specific plate (3DP) was developed using Autodesk Fusion 360 v2.0 (Autodesk Inc., United States of America), ensuring it accurately conformed to the outer surface contours of the reconstructed tibia model. The 3DP approach followed the standard workflow commonly used in patient-specific bone plate studies, involving surface reconstruction from computed tomography data, contour fitting to the anatomical model, and screw position design.[40,41] Its purpose was to establish a representative and reproducible patient-specific design reference for comparison with the GD method. The design process began with sketching the outer boundary of the plate from a posterior view,

positioned 18 mm below the top of the tibial plateau. The plate measured 106 mm in length, with a width of 32 mm proximally and 16 mm distally in the T-shaped section. This sketch was extruded toward the tibia to capture the natural surface geometry of the bone, forming the external profile of the insertion area. The surface was then thickened to 4.5 mm, completing the geometric design of the plate. The screw hole configuration was replicated from the CP to maintain consistency in evaluations. The final design of the 3DP is shown in Figure 1B, illustrating its alignment with the tibia's natural contours and its suitability for addressing the simulated fracture.

2.2.3. Patient-specific plate design via generative design

The GD-designed patient-specific bone plate (GDP) was also developed using Fusion 360 v2.0 (Autodesk Inc., United States of America). The process began by creating screw holes with a thickness of 4.5 mm and specific configurations on the plate. These holes were extruded outward by 2 mm to form preserved geometry, serving as fixed features during the GD process. To achieve the final plate design, GD iteratively connected these features under predefined constraints.

To ensure a precise fit and effective biomechanics, geometric and mechanical constraints were carefully defined. The proximal tibial surface was designated as obstacle geometry to prevent implant penetration into the cortical surface. A boundary constraint zone was designed to represent the plate's outer contour, ensuring appropriate shape and thickness. Additionally, a curved thickness constraint layer adjacent to the tibia, with a thickness of 4.5 mm, was set as an obstacle to maintain the plate's anatomical accuracy and ensure it did not exceed the design thickness of 4.5 mm. Cylindrical geometries were also added to simulate screws passing through the plate and into the bone, ensuring proper alignment of the screw holes. These geometric settings are shown in Figure 2. A 750 N compressive load, defined as described in **Section 2.3**, represented the typical biomechanical loading experienced by the tibia during normal gait. A wall thickness of 1.5 mm was preserved around the screw holes to maintain structural integrity while enabling lightweight optimization. The maximum overhang angle of 65° and a layer thickness of 0.8 mm reflected the buildability limits of metal powder-bed fusion, preventing the generation of geometries that would require extensive support or risk printing defects. The design objective of minimizing mass further promoted a lightweight yet mechanically robust plate suitable for load-bearing and long-term implantation. All mechanical constraints, including load-bearing capacity, objectives, and manufacturing methods, were specified to meet biomechanical requirements, as summarized in Table 1. This approach generated a set of patient-specific plates tailored to the individual's anatomy and structural requirements. Specifically, three design variants were produced, each incorporating minor differences in geometry that led to variations in predicted mechanical performance. Among the three variants, the design with the highest safety factor was identified as the most reliable option and was therefore selected as the generative GDP for subsequent fabrication and experimental testing.

2.3. Finite element analysis for early design evaluation

To rapidly evaluate the design outcomes at the early stage, finite element analysis (FEA) was applied prior to manufacturing the physical prototypes for experimental testing. The FEA served as a concept-screening tool to qualitatively compare stress distribution and displacement patterns among the plate designs.

The models were developed from the parametric computer-aided design model of the SSM tibia and the three patient-specific bone plates in Fusion 360 v2.0 (Autodesk Inc., United States of America). The bone fragments and implants were assembled to replicate the implantation configuration before FEA modeling. The screws were represented as cylinders with a diameter of 5 mm and merged with the plate to approximate the threaded connection between the screw head and the plate.

For the boundary and loading conditions, the distal section of the tibia was fixed to ensure stability. A total knee joint reaction force of approximately three times bodyweight during single-leg stance was considered, and the load was distributed between the medial plateau (55%) and the lateral plateau (45%).[42,43] A vertical compressive point load of 750 N was applied to the lateral region of the tibial plateau, representing the lateral share of the total reaction force. This condition simulated the single-leg stance of a 55 kg individual, which is clinically relevant for assessing fixation stability.

The bone plates were assigned Ti6Al4V material properties, a titanium alloy widely used in orthopedic implants due to its high strength-to-weight ratio and biocompatibility. The simulations were conducted in the Fusion 360 v2.0 (Autodesk Inc., United States of America) using the Autodesk Nastran solver. A tetrahedral mesh was generated in Fusion 360 using the default adaptive settings, with a model-based average element size of 10%, parabolic element order, and a maximum turn angle on curves of 60°. Under these identical settings, the element counts were approximately 4 million for the CP, 50 million for the 3DP, and 60 million for the GDP. The lower element number in the CP model was due to its relatively simple

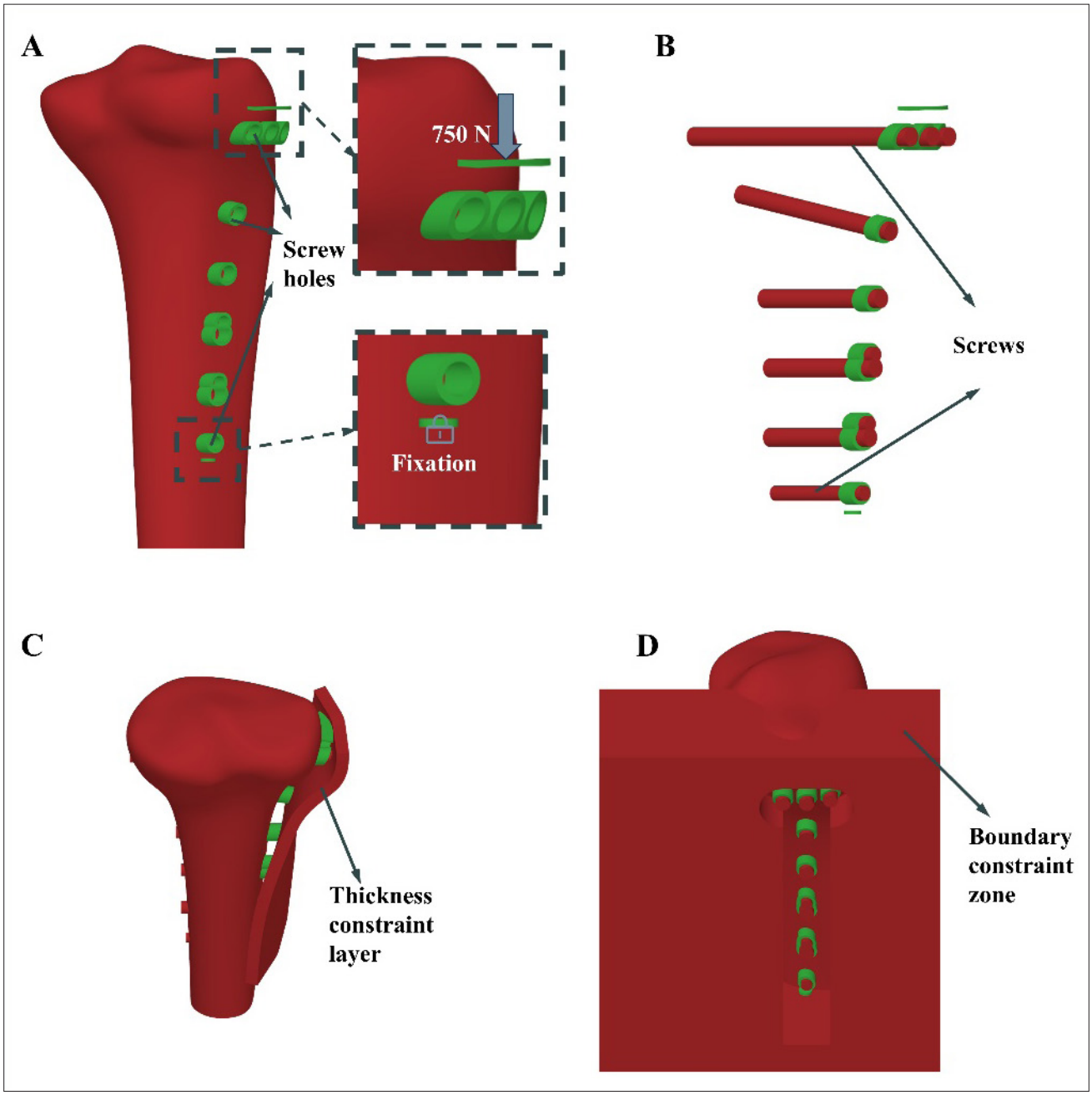

Figure 2. Design constraints and boundary conditions for the patient-specific bone plate. (A) The preserved geometry includes screw holes and fixation regions with an applied load of 750 N. The obstacle geometries are (B) screws, (C) a thickness constraint layer that defines the allowable plate thickness by maintaining a gap above the bone surface, and (D) a boundary constraint zone that limits the plate width and length during generative design.

Table 1. Parameter settings for generative design in patient-specific bone plate design

Parameter	Setting value
Preserved hole thickness	1.5 mm
Material	Ti6Al4V
Load	750 N
Design objective	Minimize mass
Manufacturing method	AM
Maximum overhang angle	65.0°
Minimum layer thickness	0.8 mm

and flat geometry, which required less mesh refinement to capture surface details. The higher element numbers in the 3DP and GDP models resulted from their more complex geometries, which led the software's model-based meshing algorithm to refine elements locally to maintain geometric accuracy and mesh quality.

2.4. Prototypes and tests

In this study, PLA prototypes were fabricated to experimentally validate the relative mechanical performance of the designed plates at the concept stage. PLA was selected for its cost-effectiveness, ease of printing, and suitability for comparative evaluation before metal fabrication. The mechanical assessment focused on two key aspects: plate quality and fixation stability. These are essential for ensuring that the bone plate provides sufficient structural strength to withstand physiological loading while maintaining stable fixation to support effective fracture healing. Three-point bending tests were performed in accordance with ASTM F382-17 to assess bending strength and stiffness.[44] Biomechanical compression tests were conducted to evaluate fixation stability under physiological conditions, as stable load transfer and minimal displacement at the fracture site are vital for promoting proper bone healing and preventing implant failure.[42,45]

2.4.1. Additive manufacturing of the tibia model and bone plates

The STL files of the tibia, including the fracture region from the virtual 3D model, were prototyped using FDM on a Prusa MINI+ 3D printer (Prusa Research a.s., Czech Republic). The skeletal model was printed in PLA + white filament with a layer resolution of 0.20 mm and a density of 100%. The finalized patient-specific bone plate designs were also converted to STL format and prepared for 3D printing using the PrusaSlicer v2.8 (Prusa Research a.s., Czech Republic). These designs were printed on the same Prusa FDM printer in PLA + white filament (Raise3D, United States of America) with a layer resolution of 0.15 mm and a density of 100%.

2.4.2. Three-point bending tests

The 3D printed PLA bone plates were subjected to three-point bending tests using a Shimadzu universal AGS-X testing machine (Shimadzu Corporation, Japan) with a 1 kN sensor. The test setup included two support rollers spaced 104 mm apart to provide stable support for the plates. A third roller applied the load at the midpoint of each plate, perpendicular to its surface, ensuring consistent loading conditions, as illustrated in Figure 3A.

The tests were conducted under displacement control at a constant rate of 1 mm/s to simulate progressive loading conditions. The load and axial displacement were continuously recorded throughout the test. Each test was terminated once the reaction force began to decrease after reaching the maximum load. Data recorded beyond the point of maximum load were excluded from the analysis to focus on the plate's peak performance and structural integrity under loading. The stiffness of each plate was determined as the slope of the linear elastic region of the load–displacement curve.

2.4.3. Biomechanical tests

The 3D-printed PLA bone plate was first fixed onto the corresponding 3D-printed fractured tibia model using stainless steel screws. Specifically, three M5 screws (40 mm in length) were inserted through the distal screw holes of the plate, and four M5 screws (80 mm in length) were inserted proximally to secure fixation. To examine the mechanical stability of the different plate designs under physiologically relevant loading, compression was primarily evaluated at 750 N, representing the typical tibial load during single-leg stance. The assembled plate–tibia construct was then mounted on a Shimadzu universal testing machine equipped with a 1 kN load cell for compression testing.

To ensure consistent alignment and test repeatability, the model was positioned on a custom-designed support base. A stainless steel load applicator, contoured to replicate the distal femur anatomy derived from the SSM, was custom-fabricated using LPBF in stainless steel (Shenzhen WeNext Technology Co., Ltd, China). This applicator was placed on the tibial plateau to simulate physiological loading representative of a standing human. The overall experimental setup is illustrated in Figure 3B.

Compression was applied under displacement control at a constant rate of 1 mm/s to simulate progressive axial loading. The load and displacement were continuously recorded throughout each test. Testing was terminated when the applied load reached the maximum sensor capacity of 1 kN. Displacement values at 500 N, 750 N, and 1000 N were recorded for comparison against the 3 mm threshold under a broader loading range, as excessive fragment displacement greater than 3 mm is

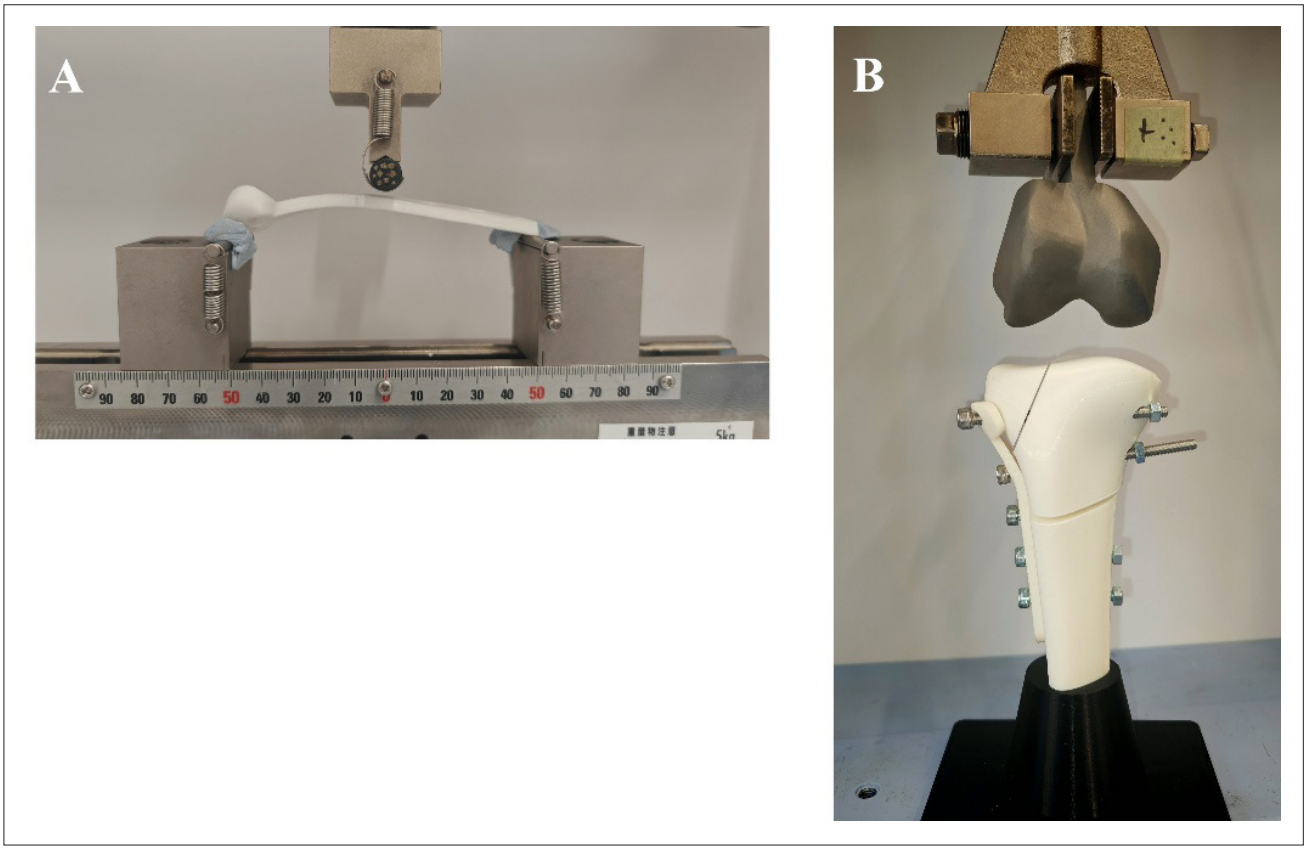

Figure 3. Experimental setup for biomechanical testing of bone plates: (A) three-point bending test and (B) biomechanical compression test.

widely recognized as a critical indicator of poor fracture healing and severe complications.[42,45–47]

2.5. Metal 3D printing for the generatively designed patient-specific bone plate

To further evaluate its mechanical performance, the final GDP was fabricated using the LPBF process on a DiMetal-280 metal AM machine (Shenzhen Jinshi 3D Printing Technology Co., Ltd., China). Ti6Al4V powder (Zhongyuan Advanced Material Co., Ltd., China) with a particle size range of 15–53 μm (D_{10} = 20 μm, D_{50} = 30 μm, D_{90} = 50 μm) was used for manufacturing the patient-specific bone plate. The printing parameters included a slicing layer thickness of 0.03 mm, laser power of 190 W, scanning spacing of 0.09 mm, and scanning speed of 1000 mm/s, with a 67° interlayer spiral filling strategy and 8 mm-wide stripe partitioning. The plate was positioned at a 45° inclination relative to the *X*-axis to enhance forming efficiency and surface quality on the downward-facing surface, with non-solid intelligent supports applied to overhangs below 30° and additional block supports placed at the lowest points. Post-processing was conducted in sequence, beginning with heat treatment (annealing) to relieve residual stress and stabilize the microstructure, followed by wire-cutting separation to remove the plate from the build substrate. The printed supports were then mechanically removed, after which the plate was precision-ground and polished to achieve the required dimensional tolerances and smoothness. Finally, surface shot peening was performed to improve surface integrity and enhance fatigue resistance. These steps ensured that the plate met the necessary dimensional accuracy, surface quality, and mechanical reliability for subsequent testing. Figure 4A presents the finalized metal generatively designed bone plate (MGDP).

Subsequently, the MGDP was subjected to biomechanical compression testing using the same setup as described for the PLA prototypes. The plate was fixed to the 3D printed tibia model with identical screw configurations, and a 750 N axial load was applied to record the corresponding displacement. This allowed a direct comparison between the PLA prototype and the metal version of the GDP under equivalent testing conditions.

Figure 4. Fabricated generatively designed plates: (A) the metal generatively designed bone plate manufactured from Ti6Al4V via laser powder bed fusion after post-processing; (B) the corresponding poly(lactic acid) prototype fabricated by fused deposition modeling for early-stage biomechanical validation.

2.6. Statistical analysis

A one-way analysis of variance (ANOVA) was performed to determine whether there were significant differences in stiffness and maximum load from the three-point bending tests, as well as displacement from the biomechanical compression tests, among the three plate designs. Post hoc analyses were performed using the Tukey honestly significant difference (HSD) test when variances were equal and the Games–Howell test when variances were unequal, based on the results of Levene's test. A significance level of 0.05 was used for all statistical tests. Statistical analysis was conducted using SPSS Statistics v27.0 (IBM Corp., United States of America).

3.Results

The final designs of the CP, 3DP, and GDP plates are presented in Figure 5, providing a visual comparison of the three design approaches prior to mechanical and biomechanical evaluation.

3.1. Finite element analysis

The FEA results, shown in Figure 6, illustrate the stress and displacement distributions of the plate–bone system for the three plate designs under a 750 N load. All designs remained within the material's ultimate strength and the 3 mm displacement threshold for bone fragments. In all cases, the maximum von Mises stress was localized in the central region of the plate. Implantation of the plates reduced stress concentrations in the tibia, helping to avoid excessive loading in the bone. All three designs met the basic structural and fixation requirements for a bone plate under the simulated loading condition.

3.2. Three-point bending test results of poly(lactic acid) prototypes

The three-point bending test results for the three plate designs are shown in Figure 7, which presents the mean load–displacement curves for the 3DP, CP, and GDP plates ($n = 5$) with error bars representing one standard deviation. The numerical values for stiffness and maximum load are summarized in Table 2. Both patient-specific designs (3DP and GDP) outperformed the CP plate. The 3DP plate demonstrated approximately 24% higher stiffness and 15% higher maximum load compared with CP, while the GDP plate achieved about 10% higher stiffness and 13% higher maximum load. Statistical analysis confirmed significant differences among groups ($p < 0.05$). Post hoc tests further indicated that both 3DP and GDP were superior to CP, while no significant difference was observed between GDP

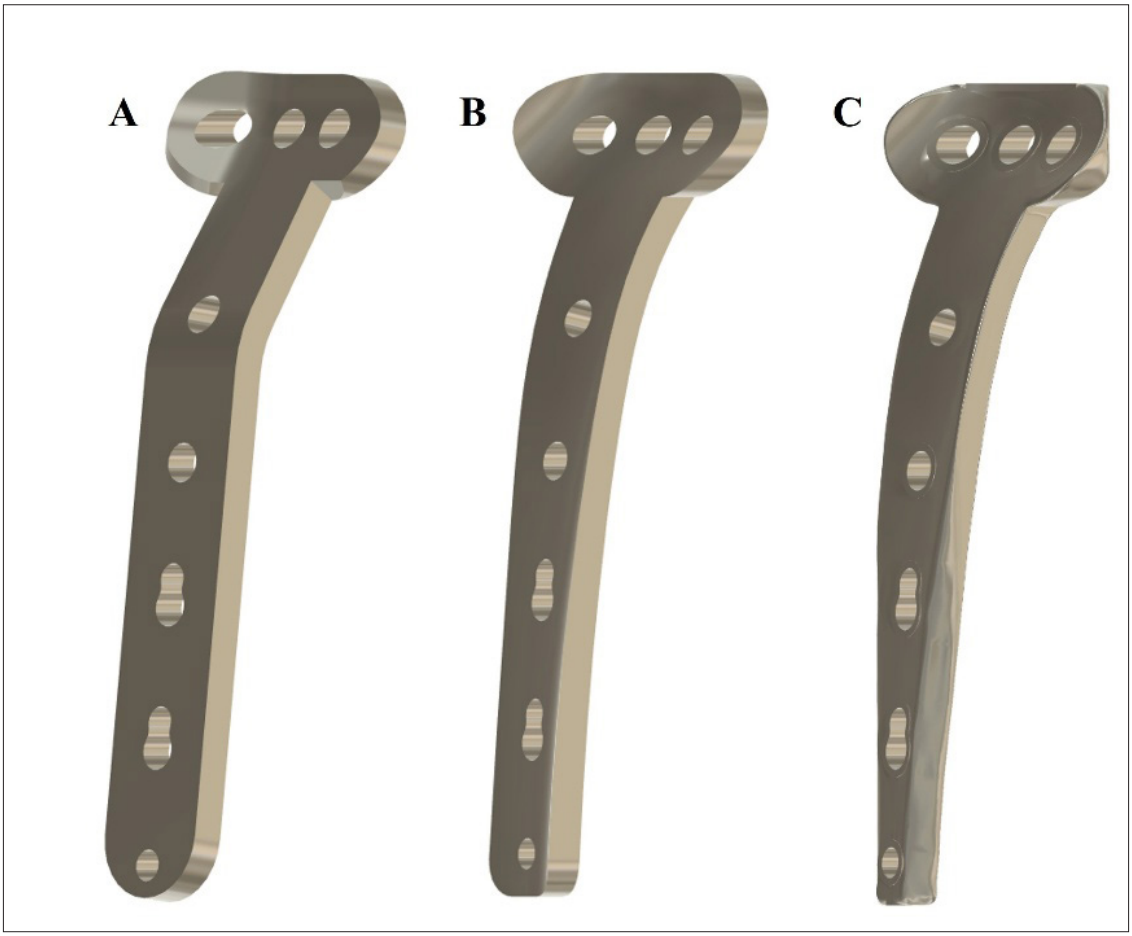

Figure 5. Final designs of the three plate types: (A) baseline plate (commercial plate), (B) patient-specific plate 3D reconstruction design plate, and (C) generatively designed patient-specific bone plate.

and 3DP ($p > 0.05$), supporting the non-inferiority of GDP relative to the established 3DP approach.

3.3. Biomechanical compression results of poly(lactic acid) and metal plates

The biomechanical compression test results are summarized in Table 3, showing the vertical displacement of the three PLA plate designs (CP, 3DP, GDP) and the metallic MGDP plate under loads of 500 N, 750 N, and 1000 N. At each load level, one-way ANOVA followed by

Tukey HSD post hoc testing revealed significant differences among the PLA designs ($p < 0.05$). Across all conditions, both GDP and 3DP provided significantly more stable fixation than CP ($p < 0.05$), with no significant difference between GDP and 3DP ($p > 0.05$). Specifically, mean displacements for the CP, 3DP, and GDP were 2.36 ± 0.16, 2.00 ± 0.08, and 1.96 ± 0.13 mm at 500 N; 2.87 ± 0.11, 2.45 ± 0.06, and 2.43 ± 0.20 mm at 750 N; and 3.09 ± 0.11, 2.65 ± 0.07, and 2.65 ± 0.22 mm at 1000 N, respectively. The MGDP demonstrated the smallest displacement across all loads, with values of 1.53 ± 0.09, 2.11 ± 0.01, and 2.39 ± 0.04 mm, remaining well below the commonly accepted clinical threshold of 3 mm.

4. Discussion

In the early stage of this study, the FEA indicated that all designed plates met the basic requirements for fixation stability and structural safety, supporting their progression to the prototype fabrication and manufacturing stages. This analysis functioned as a preliminary screening step within the overall workflow, allowing rapid, qualitative assessment of stress distribution and displacement patterns before committing resources to physical testing. Such a preliminary evaluation is valuable for identifying potential mechanical concerns and confirming that each design concept is fundamentally viable. However, the FEA modeling assumed isotropic Ti6Al4V material properties and did not incorporate the anisotropy or process-specific

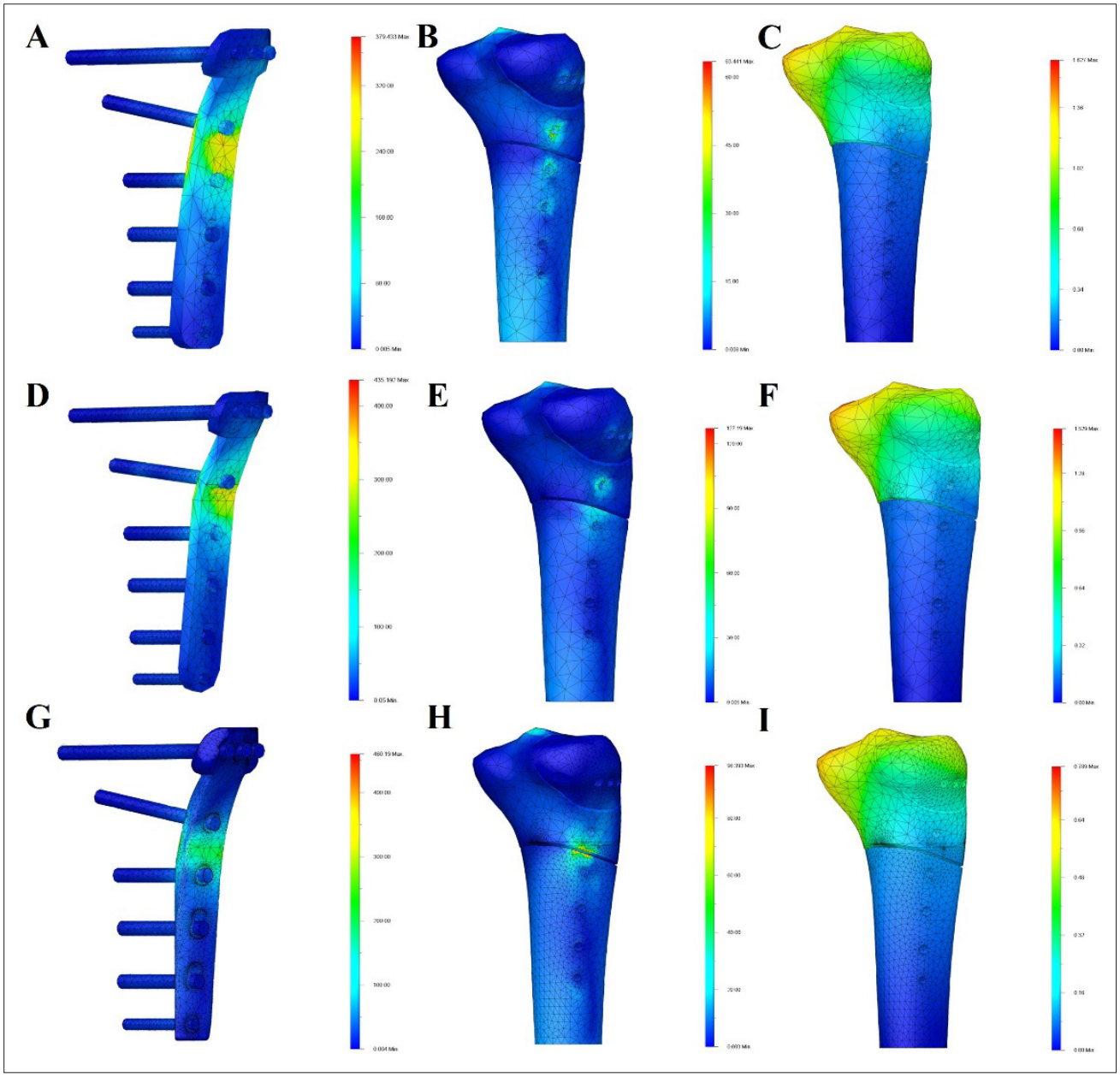

Figure 6. Biomechanical finite element analysis results of the three bone plate designs under a 750 N load. Stress distribution on (A) the CP only, (B) the tibia with the CP, and (C) displacement distribution of the tibial fragment with the CP. Stress distribution on (D) the 3DP only, (E) the tibia with the 3DP, and (F) displacement distribution of the tibial fragment with the 3DP. Stress distribution on (G) the GDP only, (H) the tibia with the GDP, and (I) displacement distribution of the tibial fragment with the GDP. Abbreviations: CP, commercial plate; GDP, generatively designed patient-specific bone plate; 3DP, 3D reconstruction design plate.

behavior associated with FDM or LPBF manufacturing, meaning the results are not directly representative of real-world performance.[48,49] Consequently, experimental testing was essential to obtain accurate and clinically relevant data, enabling a more reliable comparison of designs and validation of their suitability for practical application.

The three-point bending test results demonstrated that both patient-specific plate designs outperformed the conventional CP in terms of stiffness and maximum load capacity, as shown in Figure 7. Table 2 indicates that both patient-specific designs (3DP and GDP) were significantly stiffer and withstood higher maximum loads than the CP plate ($p < 0.05$), while no significant difference was

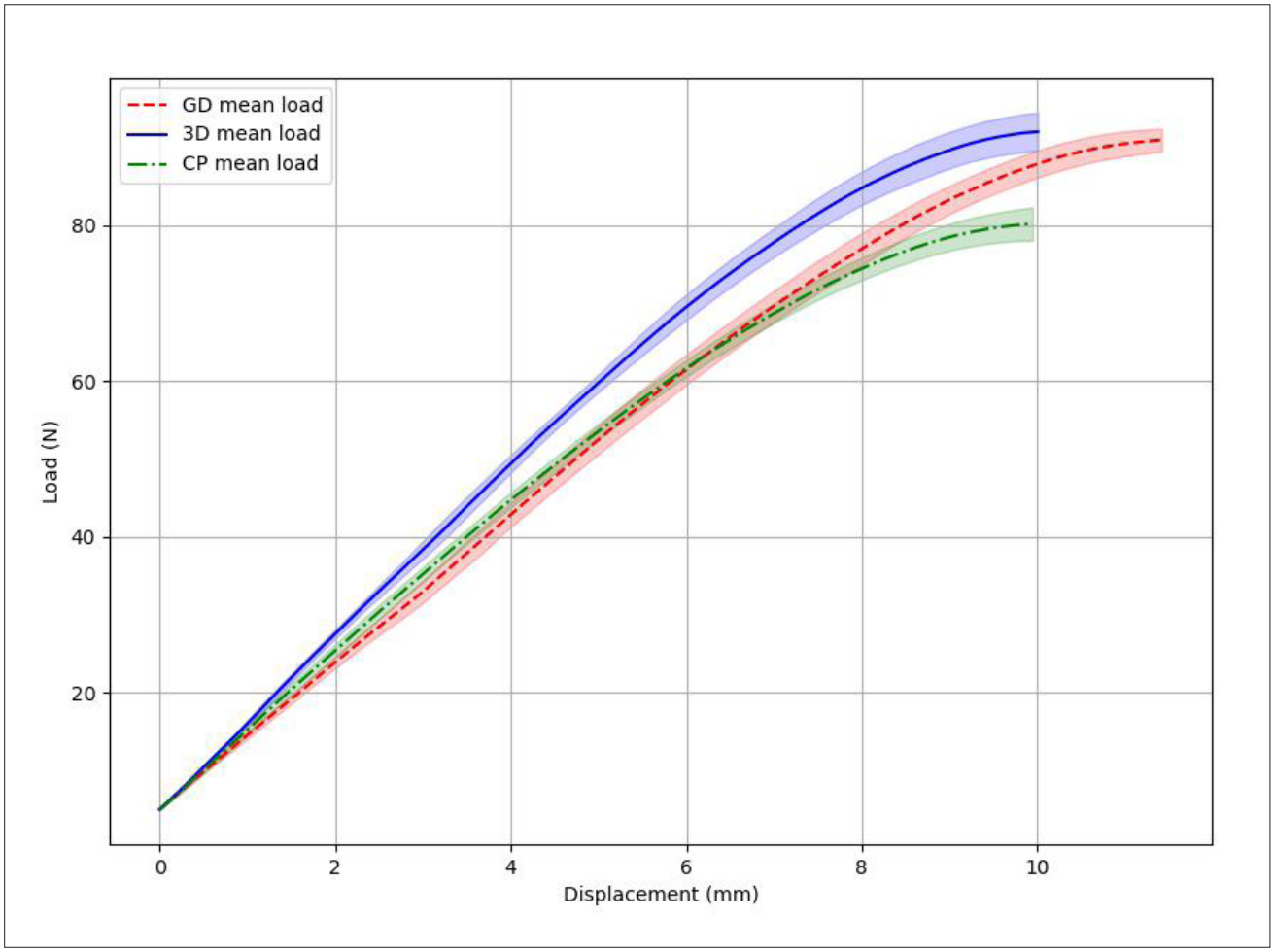

Figure 7. Load–displacement curves from three-point bending tests for the three bone plate designs (CP, 3DP, and GDP). The solid lines represent mean load values, while the shaded regions indicate one standard deviation. Abbreviations: CP, commercial plate; GDP, generatively designed patient-specific bone plate; 3DP, 3D reconstruction design plate.

Table 2. Stiffness and maximum load of CP, 3DP, and GDP designs from bending tests

Groups	Stiffness (N/mm)	Maximum load (N; $n = 5$)
CP	8.18 ± 0.25	80.45 ± 2.51
3DP	10.13 ± 0.90	92.16 ± 2.49
GDP	9.00 ± 0.45	91.21 ± 1.19

Abbreviations: CP, commercial plate; GDP, generatively designed patient-specific bone plate; 3DP, 3D reconstruction design plate.

Table 3. Vertical displacement of PLA and Ti6Al4V plates under compression loads of 500 N, 750 N, and 1000 N, tested using the same experimental setup ($n = 3$)

Design	Material/process	500 N (mm)	750 N (mm)	1000 N (mm)
CP	PLA (FDM)	2.36 ± 0.16	2.87 ± 0.11	3.09 ± 0.11
3DP	PLA (FDM)	2.00 ± 0.08	2.45 ± 0.06	2.65 ± 0.07
GDP	PLA (FDM)	1.96 ± 0.13	2.43 ± 0.20	2.65 ± 0.22
MGDP	Ti6Al4V (LPBF)	1.53 ± 0.09	2.11 ± 0.01	2.39 ± 0.04

Abbreviations: CP, commercial plate; FDM, fused deposition modeling; GDP, generatively designed patient-specific bone plate; LPBF, laser powder bed fusion; MGDP, metal generatively designed bone plate; PLA, poly(lactic acid); 3DP, 3D reconstruction design plate.

observed between 3DP and GDP. These differences may be attributed to the design characteristics of the plates. The CP features sharp transitions between its proximal and distal segments, which can create stress concentrations during bending and reduce structural stiffness. In contrast, the 3DP and GDP were designed to match the anatomical curvature of the tibia, resulting in smoother and more natural transitions that help distribute stress more evenly. This likely contributes to their superior bending performance. Between the two patient-specific designs, the 3DP performed slightly better, which may be due to its near-rectangular cross-section that offers greater resistance to bending. The GDP, although optimized for material efficiency, features a tapered, trapezoidal cross-section in the distal region. This geometry may have slightly reduced its stiffness compared with the 3DP, despite still achieving a significant improvement over the CP. The biomechanical compression test results showed that both patient-specific plate designs (GDP and 3DP) provided significantly better fixation stability compared with the conventional CP. As presented in **Table 3**, the mean displacement values under a 750 N compressive load were 2.87 mm for CP, 2.45 mm for 3DP, and 2.43 mm for GDP. Statistical analysis confirmed significant differences among the three groups ($p < 0.05$), with post hoc tests indicating that both GDP and 3DP achieved significantly lower displacement than the CP. These results suggest that anatomically conforming, patient-specific plates provide more stable fixation upon implantation by improving load transfer and minimizing micromotion at the fracture site. The enhanced stability can be attributed to the improved contact between the plate and bone surface, reducing stress concentration and promoting more uniform force distribution.[22,40,50] At 500 N and 1000 N, a similar trend was observed, with both patient-specific designs showing smaller displacements than the CP and no significant difference between GDP and 3DP. Notably, at 1000 N, the CP displacement exceeded 3 mm, indicating fixation instability, whereas both patient-specific designs remained within the clinically acceptable range, further supporting their superior mechanical reliability under higher loading conditions.

The experimental results from the bending and compression tests showed similar performance trends, with the CP consistently identified as the weakest performer. Both GDP and 3DP demonstrated improved mechanical stability compared with the CP, with GDP consistently exhibiting the lowest displacement in compression tests and 3DP achieving the highest stiffness in the three-point bending tests. Although PLA does not replicate the mechanical properties of metallic implants, it provides a rapid, low-cost, and accessible solution for comparative evaluation during the design phase.[17,25] PLA-based prototyping enables efficient screening of design alternatives, particularly in research and development settings where metal AM is costly and time-consuming. This approach also allows for safe, repeatable testing without requiring a clinical-grade environment, making it well-suited for iteration and optimization prior to final metal fabrication. Overall, the use of PLA supports design verification while reducing lead time and resource consumption.

GD is a computational approach in which designers define high-level constraints and performance goals, allowing algorithms to automatically generate and refine design solutions through iterative evaluation.[51–53] Unlike traditional modeling methods, which require manual adjustment of predefined geometry, GD enables broad exploration of design possibilities and can optimize multiple objectives, including mechanical strength, weight reduction, and manufacturability.[54–56] In this study, 3DP was used as a conventional method for designing patient-specific bone plates and achieved the highest stiffness and bending strength among the tested designs. The GDP, although a newer method, showed comparable fixation stability and achieved the lowest displacement in the biomechanical compression tests. These results demonstrate that GD can produce clinically acceptable outcomes while reducing material use and implant weight. Based on its high performance and design efficiency, the GDP was selected for further validation using metal AM. The MGDP was tested under a 750 N load and showed a mean displacement of 2.11 ± 0.01 mm. This value is well below the commonly accepted clinical threshold of 3 mm, confirming that GD is suitable not only for early-stage design but also for producing patient-specific implants that meet clinical standards.[22,40,50]

However, this study has several limitations. The biomechanical evaluation was simplified and did not include soft tissue structures such as ligaments and muscles, which are important for accurately simulating joint stability.[57–63] Future research could address this limitation by integrating soft-tissue constraints and healing-related biological processes into computational models. For instance, Tits and Ruffoni[58] demonstrated how tendon-to-bone interfaces can be represented using graded material transitions to capture load transfer through soft tissues, while Roland *et al.*[59] incorporated progressive callus formation and multiple healing phases in finite element simulations to mimic the mechanical environment throughout recovery. Similarly, Xu *et al.*[60] linked mechanical regulation models with fracture-healing theory to optimize plate stiffness, offering a framework to couple implant mechanics with tissue differentiation. Building

on these approaches, future modeling of patient-specific plates could incorporate ligament and muscle forces, as well as temporal changes in callus stiffness, using imaging-based anatomical data and validated mechanobiological parameters. Such models would enable a more realistic evaluation of fixation stability and healing outcomes under physiological loading conditions. In addition, the applied load was static and limited to simulating a standing condition, without accounting for dynamic or multi-axial loading scenarios encountered during activities such as walking, stair climbing, or twisting motions.[61,62] Although metal 3D printing was used to validate the GD under clinically relevant material conditions, the other plate designs were tested only in PLA, which may limit the direct comparison across designs due to differences in material properties and mechanical behavior. Furthermore, the study did not account for manufacturing constraints such as overhangs, thermal distortion, or anisotropy, which may affect printability and structural integrity.[63] Future work should include metal testing for all designs and incorporate manufacturing constraints into the design and manufacturing process.

5. Conclusion

In conclusion, this study compared the mechanical and biomechanical performance of patient-specific bone plates with a conventional commercial design. The results showed that patient-specific plates provide better anatomical fit and greater stiffness. They also offer improved stability for fracture fixation. These advantages suggest strong potential to enhance surgical outcomes and support faster, more reliable healing. Among the customized designs, the GD approach showed non-inferior fixation stability compared with the commonly used patient-specific bone plate design method, highlighting its potential to achieve biomechanically stable and clinically reliable outcomes. Although the GDP showed slightly lower stiffness, it achieved a more efficient balance between mechanical strength and overall weight. The GD process also offers a promising way to streamline the design workflow, potentially reducing dependence on engineers and shortening the time between diagnosis and surgery. In addition, FDM-printed PLA prototypes were used to evaluate the plate designs in the early development stage. While they do not fully replicate the properties of metal implants, the PLA models showed consistent trends with the FEA results, supporting their use as a practical, low-cost method for rapid design screening. This study focused on a Schatzker type VI tibial plateau fracture, one of the most complex and unstable fracture patterns. Demonstrating the effectiveness of GD-based patient-specific bone plates in such a demanding case indicates that the approach is not confined to a single fracture type. Instead, it has the potential to be adapted for a broader range of fractures and anatomical regions. With further validation, the GD workflow could provide a flexible and scalable framework for customized implant design, thereby broadening the clinical application of patient-specific solutions in orthopedic surgery.

Acknowledgments

None

Funding

This work was supported by the China Scholarship Council (Project No. 202208060391) and by the United Kingdom Research and Innovation Oversea Travel Grant (UKRI2858).

Conflict of interest

Paulo Bartolo and Fengyuan Liu are members of the Editorial Board of this journal but were not involved, directly or indirectly, in the editorial or peer-review process for this article. The other authors declare that they have no competing interests.

Author contributions

Conceptualization: Weiting Xu, Fengyuan Liu
Formal analysis: Weiting Xu
Investigation: Weiting Xu
Methodology: Weiting Xu, Fengyuan Liu
Resources: Xiaoqiang Zheng, Weiqiang Li, Di Wang
Supervision: Fengyuan Liu
Writing–original draft: Weiting Xu
Writing–review & editing: All authors

Ethics approval and consent to participate

Not applicable.

Consent for publication

Not applicable.

Availability of data

The data analyzed in this study are available from the corresponding author upon reasonable request.

References

1. Schatzker J, McBroom R, Bruce D. The tibial plateau fracture. The Toronto experience 1968–1975. *Clin Orthop Relat Res.* 1979;(138):94-104.

2. Meinberg EG, Agel J, Roberts CS, Karam MD, Kellam JF. Fracture and dislocation classification compendium—2018. *J Orthop Trauma*. 2018;32:S1. doi: 10.1097/BOT.0000000000001063

3. Wennergren D, Bergdahl C, Ekelund J, Juto H, Sundfeldt M, Möller M. Epidemiology and incidence of tibia fractures in the Swedish Fracture Register. *Injury*. 2018;49(11):2068-2074. doi: 10.1016/j.injury.2018.09.008

4. Tarazona D, Karadsheh M. Tibial Plateau Fractures - Trauma - Orthobullets. May 2024. https://www.orthobullets.com/trauma/1044/tibial-plateau-fractures?hideLeftMenu=true. Accessed October 22, 2024.

5. Reátiga Aguilar J, Rios X, González Edery E, De La Rosa A, Arzuza Ortega L. Epidemiological characterization of tibial plateau fractures. *J Orthop Surg Res*. 2022;17(1):106. doi: 10.1186/s13018-022-02988-8

6. Bormann M, Neidlein C, Gassner C, *et al*. Changing patterns in the epidemiology of tibial plateau fractures: a 10-year review at a level-I trauma center. *Eur J Trauma Emerg Surg*. 2023;49(1):401-409. doi: 10.1007/s00068-022-02076-w

7. Lowe J. Tibia (Shinbone) Shaft Fractures - OrthoInfo - AAOS. 2018. https://www.orthoinfo.org/en/diseases--conditions/tibia-shinbone-shaft-fractures/. Accessed November 5, 2023.

8. Kommuru D, Singh S, Shetty S, Kale S, Srivastava A. Treatment of proximal tibia fractures with locking compression plate: a prospective study. *Int J Res Orthop*. 2022;9(1):47-52. doi: 10.18203/issn.2455-4510.IntJResOrthop20223438

9. Egol KA, Tejwani NC, Capla EL, Wolinsky PL, Koval KJ. Staged management of high-energy proximal tibia fractures (OTA Types 41): the results of a prospective, standardized protocol. *J Orthop Trauma*. 2005;19(7):448. doi: 10.1097/01.bot.0000171881.11205.80

10. Wheeless CR. Type IV (Medial) Tibial Plateau Fractures. Wheeless' Textbook of Orthopaedics. July 22, 2020. https://www.wheelessonline.com/bones/type-iv-medial-tibial-plateau-fractures/. Accessed June 20, 2024

11. Hansen M, Pesántez R. Treatment of Complete Articular Fracture, Simple Articular, Simple Metaphyseal. 2024. https://surgeryreference.aofoundation.org/orthopedic-trauma/adult-trauma/proximal-tibia/complete-articular-fracture-simple-articular-simple-metaphyseal. Accessed November 21, 2024.

12. Hansen M, Pesántez R. ORIF - Plates Without Angular Stability for Complete Articular Fracture, Simple Articular, Simple Metaphyseal. 2024. https://surgeryreference.aofoundation.org/orthopedic-trauma/adult-trauma/proximal-tibia/complete-articular-fracture-simple-articular-simple-metaphyseal/orif-plates-without-angular-stability. Accessed June 20, 2024.

13. Giannoudis PV, Einhorn TA, Marsh D. Fracture healing: the diamond concept. *Injury*. 2007;38:S3-S6. doi: 10.1016/S0020-1383(08)70003-2

14. Brouwer de Koning SG, de Winter N, Moosabeiki V, *et al*. Design considerations for patient-specific bone fixation plates: a literature review. *Med Biol Eng Comput*. 2023;61(12):3233-3252. doi: 10.1007/s11517-023-02900-4

15. Dobbe JGG, Peymani A, Roos HAL, Beerens M, Streekstra GJ, Strackee SD. Patient-specific plate for navigation and fixation of the distal radius: a case series. *Int J CARS*. 2021;16(3):515-524. doi: 10.1007/s11548-021-02320-5

16. Huiskes R, Weinans H, van Rietbergen B. The relationship between stress shielding and bone resorption around total hip stems and the effects of flexible materials. *Clin Orthop Relat Res*. 1992;(274):124-134.

17. Al-Tamimi AA. Topology optimization of patient-specific custom-fit distal tibia plate: a spiral distal tibia bone fracture. *Appl Sci*. 2022;12(20):10569. doi: 10.3390/app122010569

18. Xu W, Nassehi A, Liu F. Metal additive manufacturing of orthopedic bone plates: an overview. *MSAM*. 2023;2(4):2113. doi: 10.36922/msam.2113

19. Javaid M, Haleem A. Current status and challenges of additive manufacturing in orthopaedics: an overview. *J Clin Orthop Trauma*. 2019;10(2):380-386. doi: 10.1016/j.jcot.2018.05.008

20. Teo AQA, Ng DQK, Lee P, O'Neill GK. Point-of-care 3D printing: a feasibility study of using 3D printing for orthopaedic trauma. *Injury*. 2021;52(11):3286-3292. doi: 10.1016/j.injury.2021.02.041

21. Tilton M, Lewis GS, Bok Wee H, Armstrong A, Hast MW, Manogharan G. Additive manufacturing of fracture fixation implants: design, material characterization, biomechanical modeling and experimentation. *Addit Manuf*. 2020;33:101137. doi: 10.1016/j.addma.2020.101137

22. Jo WL, Chung YG, Shin SH, Lim J hak, Kim MS, Yoon DK. Structural analysis of customized 3D printed plate for pelvic bone by comparison with conventional plate based on bending process. *Sci Rep*. 2023;13(1):10542. doi: 10.1038/s41598-023-37433-1

23. Wang C, Chen Y, Wang L, *et al*. Three-dimensional printing of patient-specific plates for the treatment of acetabular fractures involving quadrilateral plate disruption. *BMC Musculoskelet Disord*. 2020;21(1):451. doi: 10.1186/s12891-020-03370-7

24. Briard T, Segonds F, Zamariola N. G-DfAM: a methodological proposal of generative design for additive manufacturing in the automotive industry. *Int J Interact Des Manuf*. 2020;14(3):875-886.

doi: 10.1007/s12008-020-00669-6

25. Baumgartner D, Schramel JP, Kau S, *et al*. 3D printed plates based on generative design biomechanically outperform manual digital fitting and conventional systems printed in photopolymers in bridging mandibular bone defects of critical size in dogs. *Front Vet Sci*. 2023;10:1165689. https://www.frontiersin.org/articles/10.3389/fvets.2023.1165689. Accessed November 30, 2023

26. Kanagalingam S, Dalton C, Champneys P, *et al*. Detailed design for additive manufacturing and post processing of generatively designed high tibial osteotomy fixation plates. *Prog Addit Manuf*. 2023;8(3):409-426. doi: 10.1007/s40964-022-00342-2

27. Cheng M, Nayak A, Leung YY. A semi-automated design workflow for patient-specific implants in orthognathic surgery using generative design. *Int J Oral Maxillofac Surg*. 2025;54(12):1195-1200. doi: 10.1016/j.ijom.2025.03.011

28. Dewey MJ, Chang RSH, Nosatov AV, *et al*. Generative design approach to combine architected Voronoi foams with porous collagen scaffolds to create a tunable composite biomaterial. *Acta Biomater*. 2023;172:249-259. doi: 10.1016/j.actbio.2023.10.005

29. Alvarado-Moreno C, Beltrán-Fernández JA, González Rebattú M, Hermida Ochoa JC. Generative design for a case of tumoral resection, reconstruction of the mandibular continuity. In: Öchsner A, Altenbach H, eds. *Engineering Design Applications VII*. Switzerland: Springer Nature; 2025:235-241. doi: 10.1007/978-3-031-84346-4_17

30. Keast M, Bonacci J, Fox A. Geometric variation of the human tibia-fibula: a public dataset of tibia-fibula surface meshes and statistical shape model. *PeerJ*. 2023;11:e14708. doi: 10.7717/peerj.14708

31. Kote V, Pant A, Templin T, Frazer L, Eliason T, Nicolella DP. Personalized tibial strain prediction: feasibility of a novel approach using markerless motion capture and statistical shape models. *J Biomech Eng*. 2025;147(12):121005. doi: 10.1115/1.4069774

32. Cai X, Wu Y, Huang J, Wang L, Xu Y, Lu S. Application of statistical shape models in orthopedics: a narrative review. *Intell Med*. 2024;4(4):249-255. doi: 10.1016/j.imed.2024.05.001

33. van Veldhuizen WA, van der Wel H, Kuipers HY, *et al*. Development of a statistical shape model and assessment of anatomical shape variations in the hemipelvis. *J Clin Med*. 2023;12(11):3767. doi: 10.3390/jcm12113767

34. Thiart M, Ikram A, Lamberts RP. How well can step-off and gap distances be reduced when treating intra-articular distal radius fractures with fragment specific fixation when using fluoroscopy. *Orthop Traumatol Surg Res*. 2016;102(8):1001-1004. doi: 10.1016/j.otsr.2016.09.005

35. Albayrak K, Misir A, Alpay Y, Buyuk AF, Akpinar E, Gursu SS. Effect of fracture level on the residual fracture gap during tibial intramedullary nailing for tibial shaft fractures. *SICOT J*. 2023;9:26. doi: 10.1051/sicotj/2023023

36. Meeson R, Moazen M, Sanghani-Kerai A, Osagie-Clouard L, Coathup M, Blunn G. The influence of gap size on the development of fracture union with a micro external fixator. *J Mech Behav Biomed Mater*. 2019;99:161-168. doi: 10.1016/j.jmbbm.2019.07.015

37. Kim TH, Heo YM, Kim KK, *et al*. Fracture gap and working length are important actionable factors affecting bone union after minimally invasive plate osteosynthesis for the treatment of simple diaphyseal or distal metaphyseal tibia fractures. *Orthop Traumatol Surg Res*. 2024;110(2):103770. doi: 10.1016/j.otsr.2023.103770

38. Liao B, Sun J, Xu C, *et al*. A mechanical study of personalised Ti6Al4V tibial fracture fixation plates with grooved surface by finite element analysis. *Biosurf Biotribol*. 2021;7(3):142-153. doi: 10.1049/bsb2.12019

39. DePuy Synthes. LCP™ Proximal Tibia Plate (3.5 and 4.5 mm) | DePuy Synthes. J&J MedTech. 2025. https://www.jnjmedtech.com/en-US/product/lcp-proximal-tibia-plate. Accessed March 12, 2025.

40. Assink N, Oldhoff MGE, Ten Duis K, *et al*. Development of patient-specific osteosynthesis including 3D-printed drilling guides for medial tibial plateau fracture surgery. *Eur J Trauma Emerg Surg*. 2024;50(1):11-19. doi: 10.1007/s00068-023-02313-w

41. Steffen C, Sellenschloh K, Willsch M, *et al*. Patient-specific miniplates versus patient-specific reconstruction plate: a biomechanical comparison with 3D-printed plates in mandibular reconstruction. *J Mech Behav Biomed Mater*. 2023;140:105742. doi: 10.1016/j.jmbbm.2023.105742

42. Ren W, Zhang W, Jiang S, *et al*. The study of biomechanics and clinical anatomy on a novel plate designed for posterolateral tibial plateau fractures via anterolateral approach. *Front Bioeng Biotechnol*. 2022;10. doi: 10.3389/fbioe.2022.818610

43. Le Quang H, Schmoelz W, Lindtner RA, Schwendinger P, Blauth M, Krappinger D. Biomechanical comparison of fixation techniques for transverse acetabular fractures – single-leg stance vs. sit-to-stand loading. *Injury*. 2020;51(10):2158-2164. doi: 10.1016/j.injury.2020.07.008

44. ASTM International. *ASTM F382-17. Standard specification and test method for metallic bone plates*. West Conshohocken, PA: ASTM International; 2017 doi: 10.1520/F0382-17

45. Feng W, Fu L, Liu J, Qi X, Li D, Yang C. Biomechanical evaluation of various fixation methods for proximal extra-articular tibial fractures. *J Surg Res*. 2012;178(2):722-727. doi: 10.1016/j.jss.2012.04.014

46. Teo AQA, Ng DQK, Ramruttun AK, O'Neill GK. Standard versus customised locking plates for fixation of Schatzker II tibial plateau fractures. *Injury*. 2022;53(2):676-682. doi: 10.1016/j.injury.2021.11.051

47. Samsami S, Pätzold R, Neuy T, *et al*. Biomechanical comparison of 2 double plating methods in a coronal fracture model of bicondylar tibial plateau fractures. *J Orthop Trauma*. 2022;36(4):e129. doi: 10.1097/BOT.0000000000002257

48. Ngo TD, Kashani A, Imbalzano G, Nguyen KTQ, Hui D. Additive manufacturing (3D printing): a review of materials, methods, applications and challenges. *Compos B Eng*. 2018;143:172-196. doi: 10.1016/j.compositesb.2018.02.012

49. Liu S, Shin YC. Additive manufacturing of Ti6Al4V alloy: a review. *Mater Des*. 2019;164:107552. doi: 10.1016/j.matdes.2018.107552

50. Vancleef S, Wesseling M, Duflou JR, Nijs S, Jonkers I, Vander Sloten J. Thin patient-specific clavicle fracture fixation plates can mechanically outperform commercial plates: an in silico approach. *J Orthop Res*. 2022;40(7):1695-1706. doi: 10.1002/jor.25178

51. Barbieri L, Muzzupappa M. Performance-driven engineering design approaches based on generative design and topology optimization tools: a comparative study. *Appl Sci*. 2022;12(4):2106. doi: 10.3390/app12042106

52. Frazer J. Creative design and the generative evolutionary paradigm. In: Bentley PJ, Corne DW, eds. *Creative Evolutionary Systems*. San Francisco, CA: Morgan Kaufmann; 2002:253-274 doi: 10.1016/B978-155860673-9/50047-1

53. Tel A, Kornfellner E, Moscato F, *et al*. Optimizing efficiency in the creation of patient-specific plates through field-driven generative design in maxillofacial surgery. *Sci Rep*. 2023;13(1):12082. doi: 10.1038/s41598-023-39327-8

54. Krish S. A practical generative design method. *Comput Aided Des*. 2011;43(1):88-100. doi: 10.1016/j.cad.2010.09.009

55. Watson M, Leary M, Brandt M. Generative design of truss systems by the integration of topology and shape optimisation. *Int J Adv Manuf Technol*. 2022;118(3):1165-1182. doi: 10.1007/s00170-021-07943-1

56. Wang Z, Zhang Y, Bernard A. A constructive solid geometry-based generative design method for additive manufacturing. *Addit Manuf*. 2021;41:101952. doi: 10.1016/j.addma.2021.101952

57. Mehboob A, Barsoum I, Mehboob H, Abu Al-Rub RK, Ouldyerou A. Topology optimization and biomechanical evaluation of bone plates for tibial bone fractures considering bone healing. *Virtual Phys Prototyp*. 2024;19(1):e2391475. doi: 10.1080/17452759.2024.2391475

58. Tits A, Ruffoni D. Joining soft tissues to bone: insights from modeling and simulations. *Bone Rep*. 2020;14:100742. doi: 10.1016/j.bonr.2020.100742

59. Roland M, Diebels S, Wickert K, Pohlemann T, Ganse B. Finite element simulations of smart fracture plates capable of cyclic shortening and lengthening: which stroke for which fracture? *Front Bioeng Biotechnol*. 2024;12:1420047. doi: 10.3389/fbioe.2024.1420047

60. Xu S, Ding X, Xiong M, Duan P, Zhang H, Li Z. The optimal design of 3D-printed lattice bone plate by considering fracture healing mechanism. *Int J Numer Methods Biomed Eng*. 2023;39(3):e3682. doi: 10.1002/cnm.3682

61. Moosabeiki V, de Winter N, Cruz Saldivar M, *et al*. 3D printed patient-specific fixation plates for the treatment of slipped capital femoral epiphysis: topology optimization *vs.* conventional design. *J Mech Behav Biomed Mater*. 2023;148:106173. doi: 10.1016/j.jmbbm.2023.106173

62. Zong H, Lou B, Yuan H, *et al*. Integrating kinematic and dynamic factors with generative design for high-performance additive manufacturing structures. *Virtual Phys Prototyp*. 2025;20(1):e2501383. doi: 10.1080/17452759.2025.2501383

63. Attar H, Ehtemam-Haghighi S, Kent D, Dargusch MS. Recent developments and opportunities in additive manufacturing of titanium-based matrix composites: a review. *Int J Mach Tools Manuf*. 2018;133:85-102. doi: 10.1016/j.ijmachtools.2018.06.003